Research on Ship to Ship Channel Characteristics Based on Effect of Antenna Location in Inland Waterway at 5.9 GHz

Jing Zhang[1], Changzhen Li[1], Luyao Du[1], and Wei Chen[1]*
[1] School of Automation, Wuhan University of Technology
Wuhan, Hubei 430070 - China
[e-mail: jzcaptain@whut.edu.cn, greatchen@whut.edu.cn]
*Corresponding author: Wei Chen

Received December 16, 2019; revised April 12, 2020; accepted June 11, 2020; published August 31, 2020

Abstract

A considerable literature has recently grown up on the theme of ship wireless communications. However, much of the research up to now has been descriptive in the offshore area. There has been little quantitative analysis of wireless communication in inland waterways, which has received considerable attention lately. Until now, only the effects on inland river environment are examined. What is less clear is the nature of channel change caused by the antenna movement. Here we explore the moving ship-to-fixed-ship fading characteristics at 5.9 GHz for an inland waterway in the city center of China. The ship motion trajectory is designed in order to determine the effect of changes in the antenna position. We evaluate the channel fading characteristics of inland waterway, which are highly correlated with the distance between transmitter and receiver. We demonstrate that the line-of-sight component, as well as the components from multipath with obstruction reflections, contributes largely to the mean power gap. Our findings reveal critical ship-to-ship characteristics in inland waterway, which definitely contribute to the field of ship wireless communications.

Keywords: Channel Characteristics, Small Scale Fading, Path Loss, Antenna Location Change, Ship to Ship

http://doi.org/10.3837/tiis.2020.08.011 **ISSN : 1976-7277**

1. Introduction

With the rapid development of shipping, increasing attention has been focused on wireless channel characteristics for ship communication systems [1]. Wireless communication has a pivotal role in water transport traffic information. There is a growing body of literature recognizes that the importance of ship wireless communication. There are a number of important differences between the transmission of radio waves on the water surface and radio waves on the land. In addition to the distance and the obstacles, the absorption and reflection of radio waves by water should be considered. Consequently, much research has been performed on the effects of water surface environments (e.g. coastal and inland river environments) [2, 3]. Furthermore, much of the previous work on ship radio channel measurements is implemented in the sea environment [4-6]. The issue of Inland waterway (IW) wireless communication has received considerable critical attention.

IW wireless communication (IWWC) technology can guarantee ship-to-ship safety. Previous vehicle-to-vehicle (V2V) measurement campaigns focus exclusively on wireless propagation within specific environments [7]. However, the communication technology satisfying the needs of the ship community in for the inland waterway environment is still lacking. Recently, researchers have shown an increased interest in IWWC. IWWC is expected to offer ships data rich wireless communications, including high quality voice and video broadcasting, which can potentially guarantee real-time communication between ship users and the waterway administration during journeys. In addition, IW communication can enhance inland navigation traffic safety.

However, the determination of IWWC is technically challenging, the characteristics of ship channel propagation are distinct from other cellular channel profiles, particularly within the time and frequency domains. For example, a multipath fading channel model based on measured data in the Greek Aegean Sea [8]. It describes unique wireless propagation in sea environment which is distinctively different from that of IW environment channel systems. Experiments in [9] demonstrated that transmission distance has a significant impact on the power delay profile (PDP). This implies that under certain conditions, extended distances will reduce frequency fading within the sea environment. Furthermore, [4] proposed several marine communication propagation characteristics, yet most were based on an ocean environment, thus limiting the feasibility of such characteristics for inland waterway research. Such expositions are unsatisfactory because they lacked the experimental data analytics to research the IWWC much further. In order to improve our understanding on the mechanisms underlying the stationarity of IW channels, the current study investigates channel characteristics of a moving ship based on experimental measurements.

This paper highlights the importance of the reliable and realistic channel measurement is the enabling foundation to review any wideband digital mobile radio system for IWWC. There are two primary aims of this study: 1. To investigate IWWC channel characteristic. 2. To ascertain the influence of Antenna Location

This dissertation follows a practicalities in inland waterway, with in-depth analysis of the path loss exponent and small scale fading are developed under condition of similarity scenarios (velocity, direction, et. al) at 5.9 GHz. Meanwhile, Doppler features of line of sight(LOS) components are statistically studied. And also investigated the time delay characteristics respecting to the varying position when ship moving. In particular, channel characteristics such as channel gain, delay and Doppler spreads were derived from

measurement data obtained from different positions of the ship motion trajectory. Small-scale fading analysis reveals that the K-factor and power delay profile (PDP) characteristics vary significantly with the distance between the transmitter and receiver.

This paper first gives a brief overview of the inland waterway channel. The article is composed of four themed sectors. In Section II, we provide the detail of the measurement equipment and the specifications for the scenario. After that, Section III dedicates the path loss analysis used for the channel measurements, two measurement campaigns and comparison of results are given. Section IV mainly contains statistical feature analysis and crucial parameter estimations in small scale characteristics. In section V, we explain the results of RMS delay and Doppler spreads. At last, acknowledgements and conclusion are noted in Section V.

2. Environment, Equipment, and Measurements

Measurements were performed in the Wuhan section of Yangtse River, between YingWu Zhou Bridge (red dotted line in **Fig. 1**) and Wuhan Yangtze River Bridge (yellow dotted line in **Fig. 1**). The measurement environment is indicated on a satellite map in **Fig. 1**. The receiver (RX) station (yellow pin in **Fig. 1**) is located at the coordinates of 30°30′51″N, 114°17′15″E. The red arrow in **Fig. 1** indicates the ship motion trajectory, representing a ship motion along the waterway side from point A point to point B. Furthermore, h denotes the perpendicular distance from the RX to the motion trajectory, with the blue arrow showing the distance as approximately 525 meter according to Global Positioning System (GPS) measurements. Many anchored ships can be observed in the measurement area along the riverside behind the RX. In summary, the several significant channel characteristics will be affected by the wireless propagation fading during the ship moving in inland waterway.

Fig. 1. Satellite Map of Measurement Area by Google Earth

Measurements were obtained using a time-division multiplexing (TDM) channel sounder (**Fig. 2** (c) and (d)) provided by Super Radio AS of Norway to test the IW channel characteristics. As shown in **Fig. 2**, the channel sounder mainly consisted of the transmitter (TX) and RX (**Fig. 2** (a) and (b)). The parameters of the measurement setup are listed in **Table 1**. The TX antenna mounted on the ship (**Fig. 2** (b)) included an omnidirectional antenna pointed in the direction of the ship motion with a 2 dB gain. The RX was fixed on the

deck of a pontoon mooring on the riverside (**Fig. 2** (a)). A chirp signal with a 10 ns delay resolution and a 100 MHz bandwidth with a signal power of 16 dB was transmitted by the antenna. Moreover, the channel generation function h(f,t) was obtained using a Fourier transform of the channel impulse response, and the maximum supporting Doppler band was ±966.5 Hz. Based on the time structure of the TDM channel sounder, the RX could receive 833 chirps per second (T_t = 1200 μs), and each chirp signal contained 2560 samples. The remaining components of the test system included laptops, power supplies, ships, a boat pontoon, and a GPS (**Fig. 2** (c) and (d)).

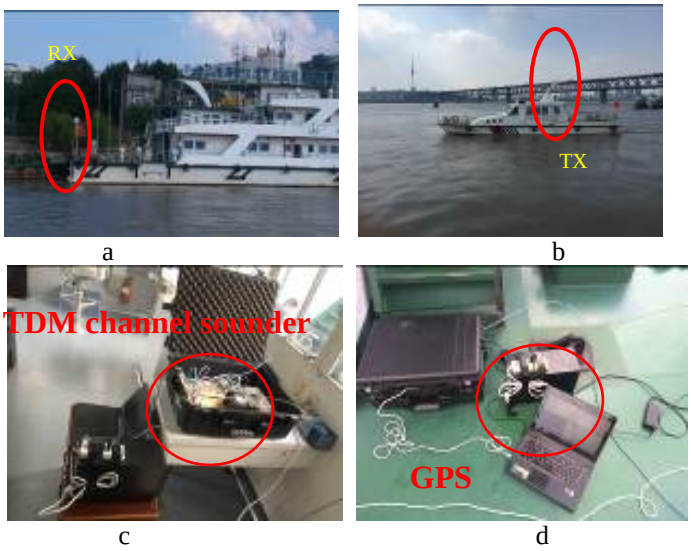

Fig. 2. a,b,c,d are photos of the propagation environments of TX and RX and channel sounder, respectively

(a) RX position on the Pontoon
(b) TX is mounted on the ship deck
(c) TDM channel sounder
(d) The remaining components of the test system

Table 1. Measurement parameters

Parameters	Values
Center frequency	5.9 GHz
Delay resolution	8.125ns
TX Beam-width elevation	±5.5°
TX antenna type	Dipole(vertical)
RX Beam-width elevation	±4°
RX Beam-width azimuth	±45°
TX height	5.0625m
RX height	4.61m

2.1 Scenario Description

In order to assess the impacts of changes in position on wireless propagation, we defined the ship movement trajectory (red arrow in **Fig. 1**) as standard (**Fig. 3**). This was done in order to distinguish the ship moving samples and to evaluate channel fading in IW. Furthermore, for a more detailed investigation, we divided the ship movement trajectory into two regions,

namely TX-C1 and TX-C2. The route from point A to point B is divided equally between TX-C1 and TX-C2. Midpoint C of this route is the nearest point to the RX, and the distance from point C to RX is h=525 m (**Fig. 3**).

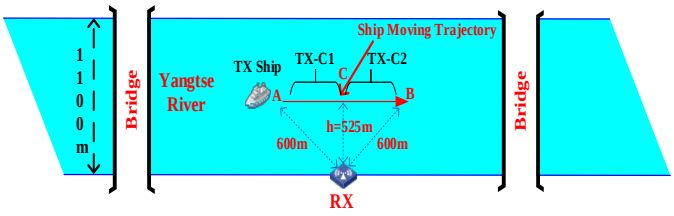

Fig. 3. Overview of the measurement by plane graph

Ichnography was used to measure and analyze the relationship between the moving ship and its direction (**Fig. 3**). More specifically, the RX was located between the two bridges and kept stationary during the measurements; v=0 m/s. From the satellite image in **Fig. 1** with the actual measurements reveals a waterway width of 1100 m, and a distance between the RX and the trajectory of point A or B of 600 m. In addition, the TX was equipped with an omnidirectional antenna mounted on the ship with a speed of $V_t \approx 5$ m/s throughout the trajectory. The water velocity in the Wuhan section in summer was assumed to be 2.5 m/s [10].

2.2 Data collection and processing

To identify the channel statistical characteristics, the channel sounder signals were converted from the frequency domain to a channel impulse response (CIR) using a Fourier transform. The existing literature on CIRs is extensive and focuses particularly on the methods for collecting CIRs [11]. For each measurement, a laptop can store the CIR values sampled by the RX, it then collects the phase of each vector sample and the PDP of each associated received signal. Using the impulse response function of Bello [11], The relationship between the channel input and output can be expressed by an impulse response function.

where $H(\tau)$ is known as the time-varying impulse response function. Where, A_i is the attenuation amplitude of path i; φ_i is the phase deviation of path i; τ_i is the time delay of path i; N is the total number of paths; δ_τ is Dirac Delta function. The characterize of the channel usually purported to represent the autocorrelation function of the impulse response.

$$H(\tau) = \sum_{i=1}^{N} A_i e^{-j\varphi_i \delta(\tau-\tau_i)} \tag{1}$$

3. Path Loss

The derivation of the path loss is determined using the measured transfer functions. From previous environment descriptions, we first compiled each measurement location channel's statistical descriptions. To determine the path loss, the time-varying PDP was derived for each time sample. For each CIR matrix, the PDP was described for each row as follows:

$$P(n,\mu) = \sum_{t=0}^{t=i} \left| M(n,m) \right|^2 \delta(\mu - m) \tag{2}$$

where n is the index of the row, μ is the index of the discrete delay, and M(n, m) is the CIR matrix that represents the element in the n^{th} row and m^{th} column. Each PDP was normalized by the strongest tap, and average the PDP was computed by averaging all the normalized PDPs in the CIR matrix. The averaged PDP (APDP) was calculated as follows [11]

$$P_h\left(t_j,\tau\right)=NAV^{-\sum_{n=0}^{NAV-1}\left|h\left(t_j+n\Delta t,\tau\right)\right|^2} \tag{3}$$

In this expression, $h\left(t_j+n\Delta t,\tau\right)$ is defined by Equation (1), and:

$$t_j=\left(0,NAV\Delta t,\ldots,\left\lfloor\frac{N_t}{NAV-1}\right\rfloor NAV\Delta t\right) \tag{4}$$

where τ is the propagation delay, NAV is the time sample value for small scale fading, and Δt is the time step. NAV was calculated as s/vΔt, where v is the velocity of the TX, and s is the wavelength that corresponds to the movement.

As the propagation distance increases, the overall path loss also increases. The channel fluctuations are affected by many factors, such as ground reflection, overwater refraction, building shadows, and additional ships between the ship being studied and the boat pontoon. These loss factors may affect the communication channel [12]. The path loss formula can be expressed as follows.

$$PL(d)=P_t+G_t+G_r-P_r-P_c \tag{5}$$

where PL(d) is the path loss at an RX-TX separation distance d, P_t is the transmission power of wireless signals without an antenna gain of 16 dB, G_t is the transmitted antenna gain, G_r is the received antenna gain, P_r is the received signal power at distance d, and P_c is the cable transmission loss, given as 6 dB. Measurements can be used to obtain the path loss values and the average path loss for each test point.

In terms of impact, it's been shown that barriers and distance reinforce each other's path loss [13]. We found that the change of received power of two groups occurs were bring by the distance change between TX and RX. **Table 2** give the statistical characteristics of path loss in whole measurement. **Fig. 4** describe the path loss of TX ship was moving under measurement. By understanding **Fig. 4**, we can increase our understanding and learn more about the path loss differences between TX-C1 and TX-C2. It could be seen that the path loss from A point to C point represented by blue line is depicted as TX-C1. Moreover, the red line, it represents path loss of TX-C2. The A, B, C point in **Fig 3** and **Fig 4** are identical. By analyzing **Fig 4** and **Table 2**, all the propagation path loss includes TX-C1 and TX-C2 from 525 meter to 600 meter. The characteristic curve of of the TX-C1 and TX-C2 path loss showed significant differences. The path loss of TX-C2 was about 7.33 dB higher than of TX-C1 on average, as shown in **Table 2**.

Fig. 4 is quite revealing in several ways. First, for TX-C2, a significant positive correlation can be observed between the path loss and distance. The path loss of TX-C1 is weaker against TX-C2 changes for the same change in distance. Furthermore, it is evident that the path loss of TX-C1 and TX-C2 exhibit differences, even for the same parameter conditions and under the same changes in distance. This may be attributed to the antenna mounting locations on the ship. More specifically, the location of the antennas may cause channel diversity and shadow fading, depending on the position of the ship. Thus, any path loss conclusions should be considered in terms of the effects of any obstacles between the TX and the RX.

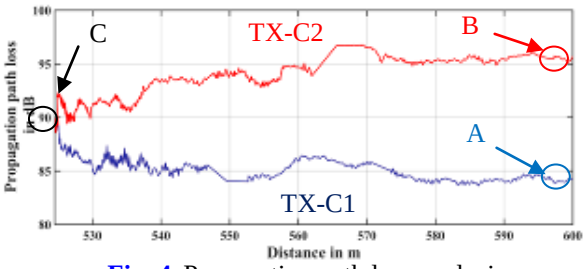

Fig. 4. Propagation path loss analysis.

One of the more significant findings to emerge from this study is that there are different of TX-C1 and TX-C2 under the same parameter conditions and the same distance change in IW channel system. Beyond this, any path loss conclusions must be regarded as the effects of obstacles between the TX and the RX.

Table 2. The Statistical Characteristics of Path Loss in whole measurement

States	Min	Max	Ave	Std
TX-C1	82.62	89.03	84.74	1.40
TX-C2	87.58	95.79	92.07	1.91

4. Small Scale Fading Characteristics

Small-scale fading is a rapid change in the amplitude, phase, or multipath delay when the radio signal is transmitted over a short time or distance [14]. Many researchers have utilized small-scale fading to measure the channel characteristics. To obtain the small-scale characteristics, the path losses were filtered from the received signals. In this article, the small-scale fading used a sliding window with a length of 20 wavelengths to study and analyze the raw data.

4.1 Amplitude Fading Distribution

The Akaike information criterion (AIC) standard was founded and developed by Japanese statistician Akio Hiroshi [15]. It is a method used to measure the goodness of a statistical model fit. The AIC information can estimate the complexity of a model and use it to compare common channel distributions, such as the Rician, Rayleigh, and Nakagami distributions [16-18]. Moreover, the AIC information can be used to obtain fitting curves of the measurement data to rule out the possibility of overfitting. Therefore, based on the smallest AIC value method, the optimum preferred model can be selected. Normally, the AIC is calculated as follows:

$$AIC = e^{\left(\frac{2k}{T}\right)} \frac{\sum_{t=1}^{T} e_t^2}{T} \tag{6}$$

where $e^{2k/T}$ is the penalty factor, and k is the number of coefficients, T is number of the sample observed. It was further assumed that the error of the model obeyed an independent normal distribution, and thus the AIC can be expressed as follows:

$$\ln AIC = \frac{2k}{T} + \ln\left(\frac{RSS}{T}\right) \tag{7}$$

where RSS is the root sum squared. If RSS is applied, it is usually represented by a normal or approximately normal distribution. The RSS is equal to the square root of the sum of the squares of the measurement statistics.

The results confirmed the association between the AIC values and the effects of various distributions on the channel propagation. **Fig. 5** below illustrates some of the main characteristics of the amplitude distribution values for these test periods. The red "×" markers denote the Rician distribution, the blue "✦" markers denote the Nakagami-m distribution, the green "★" markers denote the Rayleigh distribution, and the black "▽" markers denote the Weber distribution. The results of the AIC distribution correlational analysis are shown in **Fig. 5** (a), (b) and **Table 3**.

Fig. 5 shows that for TX-C1 and TX-C2, the AIC analysis assigns more significance to the Rician distribution compared with the other distributions. A closer inspection of **Fig. 5** reveals that the Rician distribution is located centrally within all distributions. The Rician distribution was the most prominent due to the absence of obstructions between the TX on the ship and the RX in the TX-C1 and TX-C2. Thus, there a LOS was always present between the TX and the RX. The most surprising aspect of the AIC distribution analysis is the inconsistency between TX-C1 and TX-C2.

According to the AIC analysis, for these two scenes, the Rician distribution accounts for the largest proportion in two state, as there are few ships in the inland waterway. The Rician distribution is the most obvious due to the absence of obstructions between the TX ship and RX. The Rayleigh distribution is mainly present in the absence of any direct path when radio waves cannot be directly transmitted to the RX. The Weber distribution is more complicated than the Rayleigh distribution. This is due to special path conditions in the transmission of radio waves (bridge building obscured, reflection by buildings on river side, etc) when the ship moving in the waterway. Thus, the Weber distribution also accounts for a certain proportion.

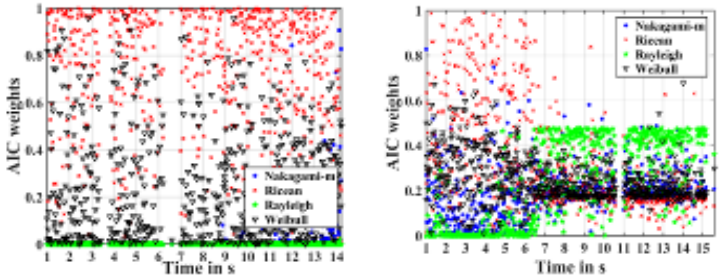

a: AIC distribution of TX-C1 b: AIC distribution of TX-C2

Fig. 5. AIC distribution

Table 3. The Proportion of Distributions in Different States

Distributions (%) / Status	**Rician**	**Rayleigh**	**Weber**	**Nakagami -m**
TX-C1	61.23	3.06	25.11	10.59
TX-C2	57.93	23.68	15.77	2.61

4.2 The Rician distribution K-Factors Analysis

The Rician distribution is a continuous probability distribution that was used to quantify the time-varying characteristics of the received signal envelope in the wireless channel. The probability density function of the Rician distribution is expressed as follows:

$$P(r)=\frac{r}{\sigma^2}e^{\left(\frac{r^2+A^2}{-2\sigma^2}\right)}\bullet I_0\left(\frac{rA}{\sigma^2}\right) \tag{8}$$

where r is the envelope of the received signal, σ^2 is the variance of the multipath components, A is the power of the main signal, and I_0 is the zeroth-order modified Bessel function of the first kind.

The K-factor is one of the most common parameters for evaluating a Rician distribution. It can be defined as the ratio of the main signal power and the variance of the multipath components as follows:

$$K = \frac{A^2}{2\sigma^2} \tag{9}$$

To better understand the K-factor, we classified the expression into the dB type as follows:

$$K = 10\log\frac{A^2}{2\sigma^2} \tag{10}$$

When A = 0, K =-∞ dB, which indicates that the multipath fading is the largest, and the Rician distribution will transform to a Rayleigh distribution. When K = ∞ dB, signal fading is not present. Moreover, if the multipath component value is very high, the K-factor value will be reduced. When LOS propagation is present in the multipath propagation, the multipath signal obeys a Rician distribution. For the Rician distribution, the K-factor defines the ratio of the power of the main signal to the variance of the multipath component. In the LOS channel, the K-factor is generally positive, whereas if there is a reflection path or NLOS channel, the K-factor becomes negative.

To distinguish the propagation processes between TX-C1 and TX-C2, the K factors of each state were calculated (**Fig. 6** and **Table 4**). Note that the K factors were estimated using the same displacement distance and motion direction. Significant differences were identified between the performances of the two states.

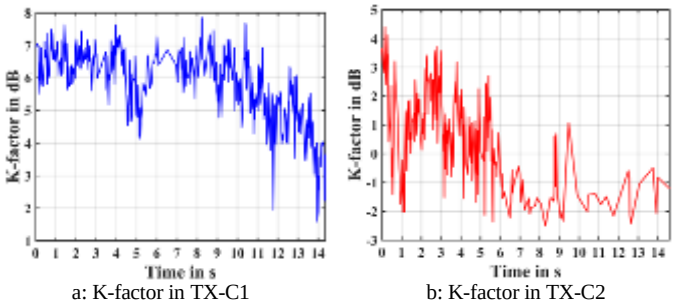

a: K-factor in TX-C1 b: K-factor in TX-C2

Fig. 6. Test scenario Rician distribution K-factor

Table 4. The Statistical Characteristics of K factor in two measurement

States	Min	Max	Ave	Std
TX-C1	1.59 dB	7.85 dB	5.78 dB	1.32
TX-C2	-2.51 dB	4.40 dB	0.55 dB	1.62

The K-factors reported in this section are estimated using a moment-based estimator. There was no observed obstacle interference to the LOS for TX-C1, yet the TX-C2 K factor was extremely low. This suggests the presence of obstacle interference to the LOS for TX-C2.

The results of the TX-C1 and TX-C2 performance comparisons are somewhat counterintuitive. This inconsistency can be attributed to several factors, including the ship motion direction and the mounting position of the TX on the ship.

4.3 Power Delay Profile

PDP is widely used to calculate the average dispersion of a transmitted signal in the time-delay domain. The term PDP refers to the power at the channel output as a function of the time delay. Previous research has established that the average and normalized PDP over a region can be regarded as stationary in the wide sense stationary (WSS). The wide sense stationary-uncorrelated scattering (WSSUS) model [19] has been applied to calculate the average delay and the root-mean-squared (RMS) delay spread extensively as a description of the frequency selection. To fully meet the requirements of the WSSUS, the time varying PDP [20] was calculated for the measurement data.

Using Equation (3), we obtained 1547 averaged PDPs for the 30 seconds measurement. These PDPs provided a measure of the spread of the received energy over time and were used to verify existence of multipath propagation. The different spread energies can also provide some information regarding the various motions in which the PDP was recorded.

Based on the APDP, we also derive the time-variant channel gain, which includes the impact of the antennas used, as follows:

$$G(t) = \sum_{\tau} P_{\tau}(t, \tau) \tag{11}$$

For the measured channel gain, we set a noise threshold, setting all components within 30 dB of the noise floor to zero to reduce the impact of noise.

The time-varying APDP and the corresponding channel gain are shown in **Fig. 7** and **Fig. 8**, respectively. These Fig.s depict the results of the average PDPs from successive WSS regions. Since the PDPs were evaluated via measurements, not from theoretical values, mathematical expressions cannot be used to describe their shape. Comparing the two states (**Fig. 7**) reveals the following conclusions. The LOS path is persistently dominant and strong, and a relatively weak path (reflection path 1) is observed parallel to the LOS component, exhibiting a long lifespan.

As shown in **Fig. 7**. The path power of TX-C1, the main strong path is reduced from −50.56 dB to −75.92 dB. The excess delays between the LOS and reflection (Path 1) paths in **Fig. 7** decrease by 1.02 μs from the beginning (excess delay: 1.72 μs) to the end (excess delay: 0.7 μs). In the TX-C2 state, a reflection path (Path 2) was evident in the 0–8 second range. the path power of the main strong path was stable in the range of -85.41 dB to -82.62 dB. In this time period, the excess delays between the LOS path and reflection path 2 in **Fig. 7** decrease by 0.07 μs from the 1st second (excess delay: 1.63 μs) to the 8th second (excess delay: 1.56 μs). It is appeared that different excess delay in same variety of space between TX and RX. The excess delay gap is on such a gigantic scale illustration that the distance change is not the main thing in influencing excess delays.

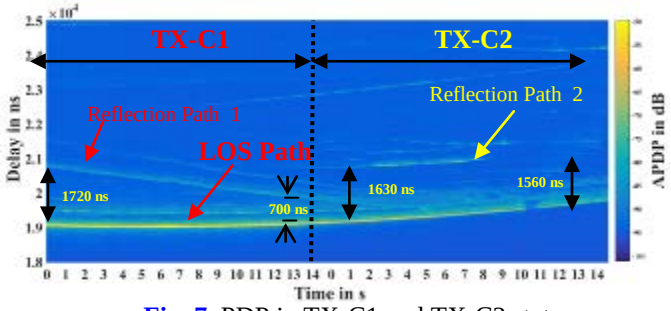

Fig. 7. PDP in TX-C1 and TX-C2 state

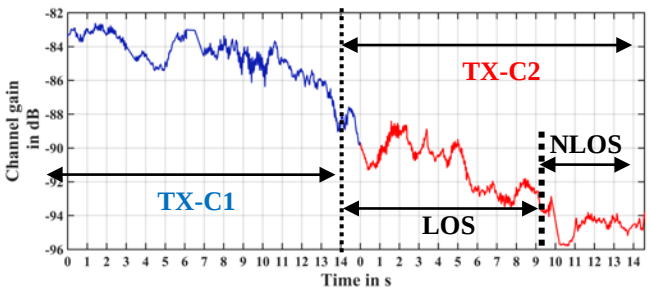

Fig. 8. Channel Gain in TX-C1 and TX-C2 state

The reflecting objects include the moving ship, vigorously rocking, waterway wave surface specular reflection, and riverside buildings; and diffuse components coming from reflections on other objects along the riverside, all of which can result in a signal delay. These surroundings are consistent with the measured results. It can be concluded that the LOS will dominate the delay domain in the waterway scenario, and that problems associated with weak reflection will be present. These reflection paths may be caused by reflections by scatterers that appear constant with respect to both the TX ship.

Differences due to the antenna gain can be best appreciated in the plots of the channel gain in **Fig. 8**. In particular, we show that different TX-RX antenna pairs result in different channel gains due to distinct position properties (i.e. same distance, different positions). The overall difference in the channel gain for the TX-RX links is higher in the TX-C1 state than in the TX-C2 state in **Table 5**. This is because in the TX-C1 state, the TX ship is moving towards the RX, unlike in the TX-C2 state, where the antenna gain of the RX is higher in the parallel direction than in the transverse direction. The channel gain for the TX-C2 state is approximately 7 dB lower than that of the TX-C1 state because the main gain of TX-C2 occurs with the TX pointing in the direction opposite to the RX direction. Therefore, the antenna gain does not have a major impact on the channel gain of the ship motion.

Table 5. The Statistical Characteristics of Channel Gain

States	Min	Max	Ave	Std
TX-C1	-89.03	-82.62	-84.73	1.39
TX-C2	-95.79	-87.58	-92.10	2.10

5. RMS Delay and Doppler Spreads Analysis

The RMS delay and Doppler spreads are also important parameters in wireless propagation. The RMS delay spread and RMS Doppler spread of the channel was indicated to describe the power spread by the channel in time and in frequency.

5.1 RMS Delay Spread

The delay spread is the difference between the last resolvable delay signal and the arrival time of the earliest delay signal [21]. The signal arriving at the receiver is a composite of each signal that has a different path and a time difference. Thus, the composite signal will exhibit a delay spread relative to the original signal in the time domain. The delay spread generally describes the temporal dispersion characteristics of a multipath channel. The root mean square delay spread is the square root of the second order matrix of the power delay distribution of the multipath channel.

The RMS delay spread describes the statistical characteristics of the multipath channel delay (12):

$$\Delta^2=\int_0^{\infty}\left(\tau-\tau_a\right)^2 P\left(\tau\right)d\tau \ . \tag{12}$$

where τ_α is the average delay, and Δ is the mean squared delay spread, which characterizes the extent of the delay spread.

Fig. 9 depicts the PDF and CDF of the RMS delay spread for the TX-C1 and TX-C2 states. The mean values of the delay spread with the typical values for each case are reported in **Table 6**.

The results from **Table 6** were somewhat expected. The lowest delay spreads were found in the TX-C1 state, mostly because of its low density of scatterers around the route of TX

antenna. Although there were similarities between TX-C1 and TX-C2, TX-C2 exhibited the largest delay spreads, possibly due to the ship motion direction and other far scatterers. Our survey revealed that when measurement ship moved past C point, the TX antenna was with its back to the RX, by looking to certain existing **Fig. 3** and TX antenna orientation.

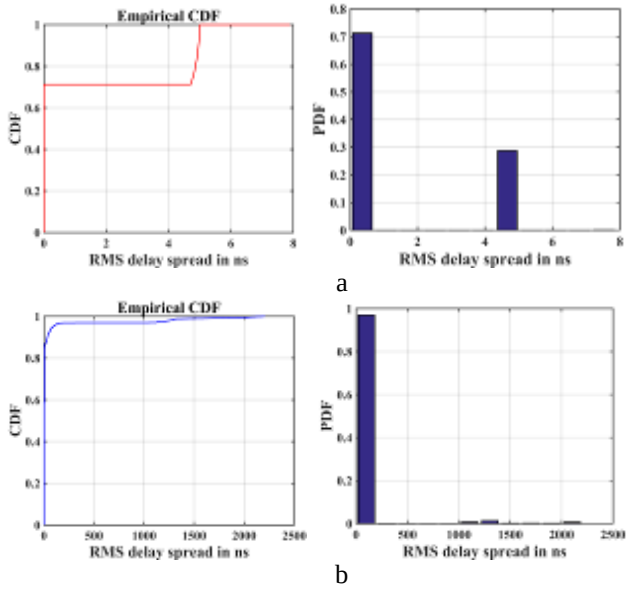

Fig. 9. Comparison of the CDF and PDF of the RMS delay spread and mean delay spread in two different motion states

CDF: cumulative density function
PDF: probability density function
(a) depict the CDF and PDF of TX-C1 state
(b) depict the CDF and PDF of TX-C2 state

Table 6. RMS Delay spread parameters for each investigated states

	Min [ns]	Max [ns]	Mean [ns]
TX-C1	0.71	7.89	1.52
TX-B2	4.72	2203	134.74

Previous studies of the RMS delay spread values have not dealt with the change of position about ship motion trajectory. The generalizability of much of the previously published research on this issue is unknown. The RMS delay spread results presented herein for low and high densities of scatterers will serve as a reference for ship moving in inland waterway environments. The PDF of the RMS delay for the TX-C1 state is 0 ns with the possibility of 70% due to the existence of a dominant component LOS. Meanwhile, the RMS delay in TX-C2 experienced the most severe multipath effects. The probability of a 0 ns RMS delay spread of the TX-C2 case was 90% because the dominant component was LOS propagation, as shown in **Fig. 9** (b). Thus, the LOS component played a leading role in the propagation processes for TX-C1 and TX-C2.

Contrary to expectations, even the same measurement distance changes can have significant difference between them. This indicates that when the ship moving in the same trajectory, reflection and the change of antenna position have a large influence on signal propagation, making the waterway situation notably different from other measurements in

typical coastal environments. Also, the RMS delay spread of ship in inland waterway is larger than the RMS delay spread of V2V in the land environment.

5.2 RMS Doppler Spread

The RMS Doppler spread is the normalized second-order central moment of the time-variant Doppler spread density. Ship movement continuously changes according to different frequency shifts. We can obtain the Doppler spread density by applying a Fourier transform on the impulse response as follows:

$$D_f\left(f_o, R_f\right) = \int_{-\infty}^{\infty} \sum_{i=1}^{N} A_i e^{-j\varphi_i \delta(\tau-\tau_i)} e^{-i2\pi\lambda\Delta t} d\Delta t\Big|_{\Delta f=0} \tag{13}$$

Where R_f is the frequency range about observation, Δf is frequency difference.

According to the autocorrelation theorem, the time-variant transfer function of the Doppler spread is equivalent to the conjugate of the function's Fourier transform.

$$D_f\left(f_o, R_f\right) = \left|F\left\{H\left(\tau\right)\right\}\right|^2 \tag{14}$$

where F is the Fourier transform.

The measured RMS Doppler spreads are shown in **Fig. 10**. Note that we assume that the TX ship maintained a continuous speed to verify the impacts of the ship motion on the IW channel. Although measurements were performed under the same conditions (velocity and direction of motion) during the whole test, TX movements will still result in large differences in the RMS Doppler spread when the multipath components arrive at the RX. We can clearly observe the changes in the Doppler spread for the two states increase consistently (**Fig. 10**). However, this growth trend is not equal to the Doppler effect.

The left part of **Fig. 10** demonstrates the Doppler spectrum in TX-C1. More specifically, it reveals that at the starting point (TX is directly moving to RX), the Doppler frequency become larger as distance between TX and RX decreases. Point C declared an end to the period of TX-C1 as well as the period of TX-C2 begin. After point C (TX is moving away from RX), the Doppler frequency exhibits a consistent growth.

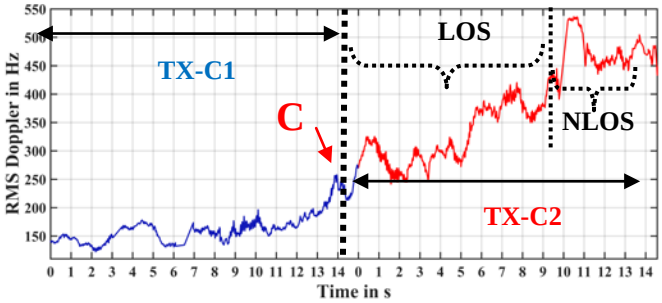

Fig. 10. RMS Doppler spreads

Furthermore, the maximum values of the TX-C1and TX-C2 Doppler spectrum generally occur in the final period. For TX-C1, we observe a relatively constant RMS Doppler spread within 145-200 Hz until the 13th second. Similarly, for TX-C2, the RMS Doppler spread value exhibits a stable trend before the 10th second. Moreover, we can clearly observe a strong Doppler component from 10 to 11 seconds, which contributes to the increase in the RMS Doppler spread. After the 11th second, the strong RMS Doppler spread disappears, with more Doppler components exhibiting stability.

The RMS Doppler spreads are observed to be proportional to the distance variations between the TX and RX. This is due to the channel fading induced by position changes, which is somewhat expected [21]. However, the observed difference between TX-C1and TX-

C2 in this study was significant. In particular, when the TX antenna moved to face the RX, the value of the Doppler spectrum grew at an inverse proportion to the distance from the TX to the RX. Conversely, when the TX antenna moved away from the RX, the TX antenna did not directly face the RX, with Doppler spectrum values proportional to the increased distance between TX and RX. Moreover, the sharp fluctuations of the Doppler components can be attributed to the switch between LOS and NLOS.

6. Conclusion

The main aim of the current study was to determine whether motion trajectory changes impact the statistics of multiple locations during ship movements in inland waterways. Based on the changes in distance between the TX and RX, fundamental propagation mechanisms were investigated via a real-time channel sounder at 5.9 GHz. The following conclusions can be drawn from the present study. The most obvious finding is that path loss is highly influenced by the moving direction of the ship. In particular, the power through the antenna can potentially increase by 8dB. Moreover, these are more prominent for Rician distribution in small-scale fading, because of the presence of no obstacles between the TX and RX. In the K factor profiles, the mean values of the measurements of the two states differed by up to 5 dB due to obstacle interference. Furthermore, results reveal that different positions in the ship motion trajectory will significantly affect the excess delays of the wireless propagation. Value deviations of excess delays were observed to be 0.95 μs between the two states for similar ship movements, depending on changes in the antenna position within the TX and RX. RMS delay and Doppler spread analysis revealed that the wireless propagation under investigation was affected by antenna shifts due to the direction of the moving ship. Therefore, the effect of the position change on the Doppler frequency in IW channel is non-negligible. Notwithstanding the relatively limited sample, this research offers valuable insights into ship antenna moving at different positions on the track. This research has thrown up many questions in need of further investigation about radiation angle of antenna. The findings of this study have a number of important implications for ship to ship wireless propagation in inland waterway practice.

Acknowledgment

The authors would like to express their sincere thanks to the Super Radio AS Oslo Norway for providing their 5.9 GHz measurement equipment. The authors also appreciate for the supports of the Wuhan University of Technology. This work is supported by Young Scientists Fund of National Natural Science Foundation of China (no. 61701356).

References

[1] HA Xia, “Research on data transmission technology of ship-shore communication” *Ship Science and Technology*, Vol. 38, No.3 A, pp. 121–123, Mar. 2016. Article (CrossRef Link).

[2] S. Gan, S. Liang, K. Li, J. Deng and T. Cheng, "Long-Term Ship Speed Prediction for Intelligent Traffic Signaling," *IEEE Transactions on Intelligent Transportation Systems*, vol. 18, no. 1, pp. 82-91, Jan. 2017. Article (CrossRef Link).

[3] C. Li, J. Yu, W. Chen, K. Yang and F. Li, "Shadowing Correlation and a Novel Statistical Model for Inland River Radio Channel," in *Proc. of ICC 2019 - 2019 IEEE International Conference on Communications (ICC), Shanghai, China*, pp. 1-6, 2019. Article (CrossRef Link).

[4] F. Bekkadal and K. Yang, "Novel maritime communications technologies," in *Proc. of 2010 10th Mediterranean Microwave Symposium, Guzelyurt*, pp. 338-341, 2010. Article (CrossRef Link).
[5] M. J. Lopes, F. Teixeira, J. B. Mamede and R. Campos, "Wi-Fi broadband maritime communications using 5.8 GHz band," in *Proc. of 2014 Underwater Communications and Networking (UComms), Sestri Levante*, pp. 1-5, 2014. Article (CrossRef Link).
[6] Yuwei Zhao, Jia Ren, Xun Chi, *Maritime Mobile Channel Transmission Model Based on ITM*, 3ca, Atlantis Press, 2013. Article (CrossRef Link).
[7] A. F. Molisch, F. Tufvesson, J. Karedal and C. F. Mecklenbrauker, "A survey on vehicle-to-vehicle propagation channels," *IEEE Wireless Communications*, vol. 16, no. 6, pp. 12-22, December 2009. Article (CrossRef Link).
[8] J. C. Reyes-Guerrero and L. A. Mariscal, "Experimental time dispersion parameters of wireless channels over sea at 5.8 GHz," in *Proc. of ELMAR-2012, Zadar*, pp. 89-92, 2012. Article (CrossRef Link).
[9] K. Maliatsos, P. Loulis, M. Chronopoulos, P. Constantinou, P. Dallas and M. Ikonomou, "Measurements and Wideband Channel Characterization for Over-the-sea Propagation," in *Proc. of 2006 IEEE International Conference on Wireless and Mobile Computing, Networking and Communications, Montreal, Que.*, pp. 237-244, 2006. Article (CrossRef Link)
[10] Lu Jinyou, "Review of Vellocity Distribution and Study on Velovity Distribution of Yangtze River Flow," *Journal of Yangtze River Scientific Research Institute*, 1990. Article (CrossRef Link).
[11] P. Bello, "Characterization of Randomly Time-Variant Linear Channels," *IEEE Transactions on Communications Systems*, vol. 11, no. 4, pp. 360-393, December 1963. Article (CrossRef Link).
[12] Almers, P., Bonek, E., Burr, A. et al., "Survey of Channel and Radio Propagation Models for Wireless MIMO Systems," *EURASIP Journal on Wireless Com Network*, 019070, 2007. Article (CrossRef Link).
[13] D. Vlastaras, T. Abbas, M. Nilsson, R. Whiton, M. Olbäck and F. Tufvesson, "Impact of a truck as an obstacle on vehicle-to-vehicle communications in rural and highway scenarios," in *Proc. of 2014 IEEE 6th International Symposium on Wireless Vehicular Communications (WiVeC 2014), Vancouver, BC*, pp. 1-6, 2014. Article (CrossRef Link).
[14] R. Kattenbach, "Statistical modeling of small-scale fading in directional radio channels," *IEEE Journal on Selected Areas in Communications*, vol. 20, no. 3, pp. 584-592, April 2002, Article (CrossRef Link).
[15] Akaike H., "Information Theory and an Extension of the Maximum Likelihood Principle," *Selected Papers of Hirotugu Akaike, Springer Series in Statistics (Perspectives in Statistics)*, pp. 199-213, 1998. Article (CrossRef Link).
[16] J.-. Molina-Garcia-Pardo, M. Lienard, A. Nasr and P. Degauque, "Wideband analysis of large scale and small scale fading in tunnels," in *Proc. of 2008 8th International Conference on ITS Telecommunications, Phuket*, pp. 270-273, 2008. Article (CrossRef Link).
[17] H. Feng et al., "Estimation of leaf nitrogen content of maize based on Akaike's information criterion in Beijing," in *Proc. of 2017 IEEE International Geoscience and Remote Sensing Symposium (IGARSS), Fort Worth, TX*, pp. 5057-5060, 2017. Article (CrossRef Link).
[18] J. Ding, V. Tarokh and Y. Yang, "Bridging AIC and BIC: A New Criterion for Autoregression," *IEEE Transactions on Information Theory*, vol. 64, no. 6, pp. 4024-4043, June 2018. Article (CrossRef Link).
[19] J. Conan and V. Subotic, "Bidirectional stochastic channel models are in general WSSUS," in *Proc. of 2008 IEEE 19th International Symposium on Personal, Indoor and Mobile Radio Communications, Cannes*, pp. 1-5, 2008. Article (CrossRef Link).
[20] C. Enneking and F. Antreich, "Exploiting WSSUS Multipath for GNSS Ranging," *IEEE Transactions on Vehicular Technology*, vol. 66, no. 9, pp. 7663-7676, Sept. 2017. Article (CrossRef Link).

[21] L. Bernadó, T. Zemen, F. Tufvesson, A. F. Molisch and C. F. Mecklenbräuker, "Delay and Doppler Spreads of Nonstationary Vehicular Channels for Safety-Relevant Scenarios," *IEEE Transactions on Vehicular Technology*, vol. 63, no. 1, pp. 82-93, Jan. 2014.
Article (CrossRef Link).

Jing Zhang received the B.S. and M.S. degrees in East China University of Science and Technology, China, in 2005 and 2009, respectively, where he is currently pursuing the Ph.D. degree in traffic information engineering and control with the School of Automation, Wuhan University of Technology. And he is now working in Changjing Wuhan Waterway Engineering Company. His research interests mainly include wireless channel, inland waterway communications, ship antenna.

Changzhen Li received the B.S. degree and the M.S. degree in engineering, both from Wuhan University of Technology (WHUT), Wuhan, China, in 2013 and 2017, respectively. He is currently pursuing the Ph.D. degree in traffic information engineering and control with the School of Automation, Wuhan University of Technology, Wuhan, China. His current research interests include signal processing in wireless communications, massive MIMO technology, vehicular, indoor and maritime radio channel measurements and modeling.

Luyao Du received the B.S. and M.S. degrees in engineering from the Wuhan University of Technology, Wuhan, China, in 2015 and 2018, respectively, where he is currently pursuing the Ph.D. degree in traffic information engineering and control with the School of Automation. His main research interests include vehicle-to-vehicle communication, data fusion methods, computational intelligence and its application in intelligent and connected vehicles & ships.

Wei Chen received his Ph.D. degree in information and communication engineering from the Huazhong University of Science and Technology, Wuhan, China, in 2005. In 1983, he joined Wuhan University of Technology, Wuhan, China, where he is currently a Professor and Doctoral Supervisor. In 2006, he was a visiting scientist with the Faculty of Engineering and Science, University of Agder, Grimstad, Norway. Prof. Chen is a senior member of IEEE, a senior member of China Electronics Society, a member of Communications and Navigation Standardization Technical Committee of Ministry of Transport of China, a member of Academic Committee on Communications and Navigation of China Institute of Navigation. His current research interests include channel measurement and modeling, massive MIMO technology, millimeter wave technology, satellite navigation system theory and technology application, and intelligent traffic control systems.